Ab initio translationally invariant nonlocal one-body densities from no-core shell-model theory

M. Burrows,[1] Ch. Elster,[1] G. Popa,[1] K. D. Launey,[2] A. Nogga,[3] and P. Maris[4]

[1]*Institute of Nuclear and Particle Physics, and Department of Physics and Astronomy, Ohio University, Athens, Ohio 45701, USA*
[2]*Department of Physics and Astronomy, Louisiana State University, Baton Rouge, Louisiana 70803, USA*
[3]*IAS-4, IKP-3, JHCP, and JARA-HPC, Forschungszentrum Jülich, D-52428 Jülich, Germany*
[4]*Department of Physics and Astronomy, Iowa State University, Ames, Iowa 50011, USA*

Background: It is well known that effective nuclear interactions are in general nonlocal. Thus if nuclear densities obtained from *ab initio* no-core shell-model (NCSM) calculations are to be used in reaction calculations, translationally invariant nonlocal densities must be available.

Purpose: Though it is standard to extract translationally invariant one-body local densities from NCSM calculations to calculate local nuclear observables like radii and transition amplitudes, the corresponding nonlocal one-body densities have not been considered so far. A major reason for this is that the procedure for removing the center-of-mass component from NCSM wave functions up to now has only been developed for local densities.

Results: A formulation for removing center-of-mass contributions from nonlocal one-body densities obtained from NCSM and symmetry-adapted NCSM (SA-NCSM) calculations is derived, and applied to the ground state densities of ^{4}He, ^{6}Li, ^{12}C, and ^{16}O. The nonlocality is studied as a function of angular momentum components in momentum as well as coordinate space.

Conclusions: We find that the nonlocality for the ground state densities of the nuclei under consideration increases as a function of the angular momentum. The relative magnitude of those contributions decreases with increasing angular momentum. In general, the nonlocal structure of the one-body density matrices we studied is given by the shell structure of the nucleus, and cannot be described with simple functional forms.

I. INTRODUCTION AND MOTIVATION

Recent developments of the nucleon-nucleon (NN) or three-nucleon ($3N$) interactions, derived from chiral effective field theory, have yielded major progress [1–3]. These, coupled with the utilization of massively parallel computing resources (e.g., see [4–7]), have placed *ab initio* large-scale simulations at the frontier of nuclear structure and reaction explorations. Among other successful many-body theories, the *ab initio* no-core shell-model (NCSM) approach, which has considerably advanced our understanding and capability of achieving first-principles descriptions of low-lying states in light nuclear systems [8–12], has over the last decade taken center stage in the development of microscopic tools for studying the structure of atomic nuclei. The NCSM concept combined with a symmetry-adapted (SA) basis in the *ab initio* SA-NCSM [13] has further expanded the reach to the structure of intermediate-mass nuclei [14]. The NCSM framework has been successfully extended to reactions of light nuclei at low energies (see, e.g., [15–18]) by combining the NCSM with resonating group methods. While this approach treats the many-body scattering problem completely microscopically, reactions involving heavier nuclei or reactions at higher energies are usually treated by reducing the many-body degrees of freedom to a more manageable few-body problem and thus introducing effective interactions between relevant clusters. Those effective interactions may either be phenomenologically described by fitting, e.g., scattering data, or one may attempt to extract them from structure calculations combined with

the continuum. A path along this line has recently been proposed [19] based on the coupled-cluster approach to nuclear structure.

Microscopic folding models for those effective interactions also have a long tradition. However, their main disadvantages is that they were usually constructed for closed shell nuclei using relatively simple models for the nuclear structure input (see, e.g., [20–22]). In order to open the path to account for the full microscopic structure of the clusters and employ first-principles wave functions, as those derived in the *ab initio* NCSM, it is an important first step to construct a one-body density, which is both nonlocal and translationally invariant, starting from one-body density matrix (OBDM) elements obtained from NCSM calculations. The need for nonlocal densities has been recognized in reaction theory, e.g., in treating the antisymmetrization between two localized clusters that accounts for particle exchange [23], as well as in folding calculations of microscopic optical potentials [20,22].

In this work we present a "proof-of-principle" study that focuses on obtaining translationally invariant (*ti*) nonlocal one-body densities and discuss their properties. We concentrate on the deformed oblate ^{12}C nucleus and the open-shell ^{6}Li. As examples for closed shell nuclei we consider ^{4}He and ^{16}O. The NCSM calculations employed here are carried out with the J-matrix inverse scattering potential, JISP16 [24,25]. In Sec. II we first define the nonlocal density, and then show how to remove the center-of-mass (c.m.) contribution to arrive

at a translationally invariant nonlocal density. In Sec. III, we illustrate the off-shell structure of the *ti* nonlocal density for ^{4}He, ^{6}Li, ^{12}C, and ^{16}O in momentum space as well as for ^{6}Li and ^{12}C in coordinate space. We also investigate the dependence of the nonlocality on the model space, and finally provide some more details of the nonlocal structure. We summarize in Sec. IV.

II. FORMAL CONSIDERATIONS

A. Space-fixed nonlocal densities

1. Space-fixed nonlocal one-body density in coordinate space

As a starting point we first derive a space-fixed (sf) nonlocal one-body density, $\rho_{sf}(\vec{r}, \vec{r}')$, between an initial A-body wave function $|\Psi\rangle$ and a final A-body wave function $|\Psi'\rangle$,

$$\rho_{sf}(\vec{r}, \vec{r}') = \langle \Psi' | \sum_{i=1}^{A} \delta^3(\vec{r}_i - \vec{r}) \delta^3(\vec{r}_i' - \vec{r}') | \Psi \rangle. \tag{1}$$

The many-body wave function $|\Psi\rangle$ is expanded in a basis of Slater determinants of single-particle harmonic oscillator (HO) states. Since we use sf single-particle coordinates, the wave functions and implicitly the calculated OBDM will include the c.m. that needs to be removed later. In this paper OBDM elements are calculated within the NCSM, using the JISP16 *NN* interaction [24,25]. The NCSM uses a finite set of single-particle HO states, characterized by two basis parameters, the HO energy $\hbar\omega$ and the many-body basis space cutoff $N_{\max}$, where $N_{\max}$ is defined as the maximum number of oscillator quanta above the valence shell for that nucleus.

Expanding the delta functions from Eq. (1) in terms of spherical harmonics, labeling the A-nucleon many-body eigenstates by the total angular momentum J, its projection M, and all additional quantum numbers collectively by λ, we obtain

$$\rho_{sf}(\vec{r}, \vec{r}') = \langle A\lambda' J'M' | \sum_{i=1}^{A} \frac{\delta(r_i - r)}{r^2} \frac{\delta(r_i' - r')}{r'^2} \sum_{lm} \sum_{l'm'} Y_l^m(\hat{r}_i) Y_l^{*m}(\hat{r}) Y_{l'}^{*m'}(\hat{r}') Y_{l'}^{m'}(\hat{r}_i') | A\lambda JM \rangle. \tag{2}$$

Here $\hat{r}$ represents the angular part of vector $\vec{r}$. After coupling the spherical harmonics to bipolar harmonics,

$$\mathcal{Y}_{lm}^{l_1 l_2}(\hat{r}, \hat{r}') = \sum_{m_1, m_2} \langle l_1 m_1 l_2 m_2 | lm \rangle Y_{l_1}^{m_1}(\hat{r}) Y_{l_2}^{m_2}(\hat{r}'),$$

$$Y_{l_1}^{m_1}(\hat{r}) Y_{l_2}^{m_2}(\hat{r}') = \sum_{l=|l_1-l_2|}^{l_1+l_2} \sum_{m=-l}^{l} \langle l_1 m_1 l_2 m_2 | lm \rangle \mathcal{Y}_{lm}^{l_1 l_2}(\hat{r}, \hat{r}'), \tag{3}$$

and using the Wigner-Eckart theorem, the nonlocal density becomes

$$\rho_{sf}(\vec{r}, \vec{r}') = \sum_{ll'} \sum_{K=|l-l'|}^{l+l'} (-1)^{J'-M'} \begin{pmatrix} J' & K & J \\ -M' & k & M \end{pmatrix} \mathcal{Y}_{Kk}^{*ll'}(\hat{r}, \hat{r}') \left\langle A\lambda' J'M' \left\| \sum_{i=1}^{A} \frac{\delta(r_i - r)}{r^2} \frac{\delta(r_i' - r')}{r'^2} \mathcal{Y}_K^{ll'}(\hat{r}_i, \hat{r}_i') \right\| A\lambda JM \right\rangle. \tag{4}$$

We can immediately make a simplification since in M-scheme calculations $M' = M$. Thus, the condition $-M' + k + M = 0$ in the $3j$ symbol forces k to be zero.

To further evaluate the nonlocal density, we rewrite Eq. (4) in second quantization form using α and β as final and initial single-particle HO states, denoted by the single-particle quantum numbers (n, l, j, t_z). Then $(a_\alpha^\dagger \tilde{a}_\beta)^{(K)}$, where $a_{nljmt_z} = (-1)^{j-m} \tilde{a}_{nlj-mt_z}$, represents the single-particle transition operator of rank K. Using the general expression of the matrix elements of a one-body operator $T_K = \sum_i T_{K,i}$ of rank K [26],

$$\langle \psi_f; J_f \| T_K \| \psi_i; J_i \rangle = \frac{1}{\hat{K}} \sum_{\alpha\beta} \langle \alpha \| T_{K,1} \| \beta \rangle \langle \psi_f; J_f \| (a_\alpha^\dagger \tilde{a}_\beta)^{(K)} \| \psi_i; J_i \rangle, \tag{5}$$

with $\hat{K} = \sqrt{2K+1}$ and $T_{K,1}$ being a single-particle operator, we obtain for the nonlocal density

$$\rho_{sf}(\vec{r}, \vec{r}') = \sum_{ll'} \sum_{K=|l-l'|}^{l+l'} (-1)^{J'-M} \begin{pmatrix} J' & K & J \\ -M & 0 & M \end{pmatrix} \mathcal{Y}_{K0}^{*ll'}(\hat{r}, \hat{r}') \frac{1}{\hat{K}} \sum_{\alpha\beta} \left\langle \alpha \left\| \frac{\delta(r_1 - r)}{r^2} \frac{\delta(r_1' - r')}{r'^2} \mathcal{Y}_K^{ll'}(\hat{r}_1, \hat{r}_1') \right\| \beta \right\rangle$$

$$\times \langle A\lambda' J' \| (a_\alpha^\dagger \tilde{a}_\beta)^{(K)} \| A\lambda J \rangle. \tag{6}$$

In Eq. (6), $\langle A\lambda' J' \| (a_\alpha^\dagger \tilde{a}_\beta)^{(K)} \| A\lambda J \rangle$ are reduced one-body density matrix (OBDM) elements. They are calculated using NCSM eigenstates $|A\lambda JM\rangle$ and $|A\lambda' J'M'\rangle$, and are input to our calculations. Replacing α and β by (n', l'_α, j') and (n, l_β, j), respectively, the reduced single-particle matrix element can be obtained using the HO single-particle wave functions. Note that, for simplicity, the isospin projections are dropped from the labels, for which $(t_z)_\alpha = (t_z)_\beta$, with only protons entering into calculations of charge

densities, while calculations of matter densities involve a summation over both protons and neutrons. We can thus separate and define the K-tensor dependence by

$$\rho_{ll'K}(r,r') \equiv \sum_{njn'j'} \hat{j}\hat{j}'(-1)^{l'+l+j+\frac{1}{2}+K} \begin{Bmatrix} l' & l & K \\ j & j' & \frac{1}{2} \end{Bmatrix} R_{n'l'}(r')R_{nl}(r)\langle A\lambda'J'||(a^{\dagger}_{n'l'j'}\tilde{a}_{nlj})^{(K)}||A\lambda J\rangle, \tag{7}$$

where $R_{nl}(r)$ is the radial component of the single-particle harmonic oscillator wave function (defined in Appendix A). Using Eq. (7), the matrix elements of $\rho_{sf}(\vec{r},\vec{r}')$ can be expressed as a sum over all tensors $\rho_{ll'K}(r,r')$,

$$\rho_{sf}(\vec{r},\vec{r}') = \sum_{Kll'}(-1)^{J'-M}\begin{pmatrix} J' & K & J \\ -M & 0 & M \end{pmatrix}$$
$$\times \mathcal{Y}^{*l'l}_{K0}(\hat{r},\hat{r}')\rho_{ll'K}(r,r'), \tag{8}$$

separating out the radial and angular components of the nonlocal density.

2. Space-fixed nonlocal one-body density matrix in momentum space

In order to remove the c.m. contribution, we need a momentum space representation of the nonlocal density, $\rho_{sf}(\vec{p},\vec{p}')$. We obtain it by applying a Fourier transformation to $\rho_{sf}(\vec{r},\vec{r}')$,

$$\rho_{sf}(\vec{p},\vec{p}') = \frac{1}{(2\pi)^3}\int\int \rho_{sf}(\vec{r},\vec{r}')e^{i\vec{p}\cdot\vec{r}}e^{-i\vec{p}'\cdot\vec{r}'}d^3r\,d^3r', \tag{9}$$

where a normalization factor $\sqrt{\frac{1}{(2\pi)^3}}$ is included for each integral, and

$$e^{-i\vec{p}\cdot\vec{r}} = 4\pi\sum_{Cc}Y^c_C(\hat{r})Y^{*c}_C(\hat{p})(-i)^C j_C(pr). \tag{10}$$

Using $\rho_{sf}(\vec{r},\vec{r}')$ from Eqs. (8) and (7), and the orthonormality of the spherical harmonics, $\int Y^c_C(\hat{r})Y^{*m}_l(\hat{r})d\hat{r} = \delta_{lC}\delta_{mc}$, leads to

$$\rho_{sf}(\vec{p},\vec{p}') = \sum_{Kll'}(-1)^{J'-M}\begin{pmatrix} J' & K & J \\ -M & 0 & M \end{pmatrix}$$
$$\times \mathcal{Y}^{*l'l}_{K0}(\hat{p},\hat{p}')\rho_{ll'K}(p,p'), \tag{11}$$

where the radial and angular part of the $\rho_{ll'K}(p,p')$ is given by

$$\rho_{ll'K}(p,p') = \sum_{njn'j'} \hat{j}\hat{j}'(-1)^{\frac{l-l'}{2}}(-1)^{j+\frac{1}{2}+l+l'+K} \begin{Bmatrix} l' & l & K \\ j & j' & \frac{1}{2} \end{Bmatrix}$$
$$\times R_{n'l'}(p')R_{nl}(p)\langle A\lambda'J'||(a^{\dagger}_{n'l'j'}\tilde{a}_{nlj})^{(K)}||A\lambda J\rangle. \tag{12}$$

This expression is used to calculate the densities from NCSM calculations of OBDM directly in momentum space. For completeness, the derivation of the local density directly in momentum space is given in Appendix A.

B. Translationally invariant nonlocal densities

In order to analyze the charge and mass distribution inside the nucleus and employ the nonlocal density, e.g., in reaction calculations, it needs to be translationally invariant. In NCSM

calculations in a HO basis with $N_{\max}$ truncation, as well as in the SA-NCSM, the wave function in single-particle coordinates exactly factorizes in a c.m. wave function and a ti wave function,

$$|\Psi JM\rangle = |\Psi_{ti}JM\rangle \otimes |\phi_{c.m.}0s\rangle, \tag{13}$$

which can be used to remove the c.m. contribution from the nonlocal density. If we want to extend the scheme for removing the c.m. contribution developed for local densities [27–31] to the nonlocal case, we need to carefully consider in which variables we want to work. While in Sec. II A the nonlocal density is calculated as a function of the independent momenta $\vec{p}$ and $\vec{p}'$, it is more convenient to proceed with the independent momenta

$$\vec{q} = \vec{p}' - \vec{p}, \quad \vec{\mathcal{K}} = \tfrac{1}{2}(\vec{p}' + \vec{p}). \tag{14}$$

The corresponding set of coordinate space variables is given by

$$\vec{\zeta} = \tfrac{1}{2}(\vec{r} + \vec{r}'), \quad \vec{Z} = \vec{r}' - \vec{r}, \tag{15}$$

where the displacement $\vec{Z}$ is translationally invariant, and $\vec{\zeta}$ is the average position.[1] Thus the c.m. contribution must only be associated with $\vec{\zeta}$,

$$\zeta = \zeta_{\text{rel}} + \zeta_{\text{c.m.}}. \tag{16}$$

Because of the exact factorization of the c.m. wave function and the ti wave function, the sf density can be expressed as a convolution of the ti density distribution ρ_{ti} with the c.m. density distribution $\rho_{c.m.}$ via

$$\rho_{sf}(\vec{\zeta},\vec{Z}) = \int \rho_{ti}(\vec{\zeta} - \vec{\zeta}_{c.m.},\vec{Z})\,\rho(\vec{\zeta}_{c.m.},0)\,d^3\zeta_{c.m.}. \tag{17}$$

Based on the set of variables from Eqs. (14) and (15), we use a Fourier transformation of the operator defined in Eq. (1) and the coordinates defined in Eq. (14),

$$\rho_{sf}(\vec{q},\vec{\mathcal{K}})$$
$$= \frac{1}{(2\pi)^3}\langle\Psi'J'M|\sum_{i=1}^{A}e^{-i\vec{q}\cdot(\vec{\zeta}_{\text{rel},i}+\vec{\zeta}_{c.m.})}e^{-i\vec{\mathcal{K}}\cdot\vec{Z}_i}|\Psi JM\rangle$$
$$= \frac{1}{(2\pi)^3}\langle\Psi'J'M|e^{-i\vec{q}\cdot\vec{\zeta}_{c.m.}}\sum_i e^{-i\vec{q}\cdot\vec{\zeta}_{\text{rel},i}}e^{-i\vec{\mathcal{K}}\cdot\vec{Z}_i}|\Psi JM\rangle. \tag{18}$$

In the above derivation we employed for the c.m. coordinate $\vec{R}_{c.m.} = \frac{1}{A}\sum_i\vec{r}_i$ and defined $\vec{\zeta}_{c.m.} = \frac{1}{2}(\vec{R}_{c.m.} + \vec{R}'_{c.m.})$. Using

---

[1]The variable $\vec{\zeta}$ can be identified with the spatial variable.

Eq. (13) we can separate the c.m. contribution from the intrinsic part of the nonlocal density:

$$\rho_{sf}(\vec{q},\vec{\mathcal{K}}) = \langle\phi_{\text{c.m.}}0s|e^{-i\vec{q}\cdot\vec{\zeta}_{\text{c.m.}}}|\phi_{\text{c.m.}}0s\rangle$$
$$\times \frac{1}{(2\pi)^3}\langle\Psi'_{ti}J'M|\sum_i e^{-i\vec{q}\cdot\vec{\zeta}_{\text{rel,i}}}e^{-i\vec{\mathcal{K}}\cdot\vec{Z}_i}|\Psi_{ti}JM\rangle. \tag{19}$$

We now can define the ti matrix elements for the nonlocal density as

$$\rho_{ti}(\vec{q},\vec{\mathcal{K}}) \equiv \frac{1}{(2\pi)^3}\langle\Psi'_{ti}J'M|\sum_i e^{-i\vec{q}\cdot\vec{\zeta}_{\text{rel,i}}}e^{-i\vec{\mathcal{K}}\cdot\vec{Z}_i}|\Psi_{ti}JM\rangle. \tag{20}$$

Thus, if we know the space-fixed nonlocal density as a function of the momenta $\vec{q}$ and $\vec{\mathcal{K}}$ and calculate the c.m. contribution in the $|0s\rangle$ state, we obtain the translationally invariant density.

Let us first consider the calculation of $\rho_{sf}(\vec{q},\vec{\mathcal{K}})$. In order to transform the sf nonlocal density to the coordinates $\vec{q}$ and $\vec{\mathcal{K}}$, the harmonic oscillator lengths must be transformed to $b_{\vec{q}}$ and $b_{\vec{\mathcal{K}}}$. This transformation is explicitly given in Appendix B. Then we need to express the product $R_{nl}(p)R_{n'l'}(p')\mathcal{Y}(\hat{p},\hat{p}')$ from Eq. (11) as a function of $\vec{q}$ and $\vec{\mathcal{K}}$. To do so, we use Talmi-Moshinsky transformations from $|nln'l':K\rangle$ to $|n_{\mathcal{K}},l_{\mathcal{K}},n_q,l_q:K\rangle$. Those Talmi-Moshinsky brackets only depend on the transformation parameter d, defined in Appendix B, the multipole K, and the harmonic oscillator quantum numbers (n,l,n',l'). They do not depend on M and require the energy conservation $2n'+l'+2n+l = 2n_{\mathcal{K}}+l_{\mathcal{K}}+2n_q+l_q$. Thus the radial and angular components of the wave functions transform as

$$R_{n'l'}(p')R_{nl}(p)\mathcal{Y}_{KM}^{l'l}(\hat{p},\hat{p}') = \sum_{n_q,n_{\mathcal{K}},l_q,l_{\mathcal{K}}}\langle n_{\mathcal{K}}l_{\mathcal{K}},n_q l_q:K|n'l',nl:K\rangle_{d=1}R_{n_{\mathcal{K}}l_{\mathcal{K}}}(\mathcal{K})R_{n_q l_q}(q)\mathcal{Y}_{KM}^{l_{\mathcal{K}}l_q}(\hat{q},\hat{\mathcal{K}}). \tag{21}$$

With this, the sf nonlocal density as a function of $\vec{q}$ and $\vec{\mathcal{K}}$ becomes

$$\rho_{sf}(\vec{q},\vec{\mathcal{K}}) = \sum_K \sum_{n_q l_q n_{\mathcal{K}} l_{\mathcal{K}}} \sum_{nln'l'jj'}\langle n_q l_q n_{\mathcal{K}} l_{\mathcal{K}}:K|n'l'nl:K\rangle_{d=1}(-1)^{J'-M}\begin{pmatrix} J' & K & J \\ -M & 0 & M \end{pmatrix}\mathcal{Y}_{K0}^{l_q l_{\mathcal{K}}}(\hat{q},\hat{\mathcal{K}})$$
$$\times (-1)^{\frac{l-l'}{2}}(-1)^{j+\frac{1}{2}+l+l'+K}\hat{j}\hat{j}'\begin{Bmatrix} l' & l & K \\ j & j' & \frac{1}{2} \end{Bmatrix}R_{n_q l_q}(q)R_{n_{\mathcal{K}} l_{\mathcal{K}}}(\mathcal{K})\langle A\lambda'J'||(a_{n'l'j'}^\dagger\tilde{a}_{nlj})^K||A\lambda J\rangle$$
$$= \sum_K \sum_{l_q l_{\mathcal{K}}}(-1)^{J'-M}\begin{pmatrix} J' & K & J \\ -M & 0 & M \end{pmatrix}\mathcal{Y}_{K0}^{l_q l_{\mathcal{K}}}(\hat{q},\hat{\mathcal{K}})\rho_{l_q l_{\mathcal{K}} K}(q,\mathcal{K}), \tag{22}$$

where the K-tensor component that depends on q and $\mathcal{K}$ is given by

$$\rho_{l_q l_{\mathcal{K}} K}(q,\mathcal{K}) \equiv \sum_{n_q n_{\mathcal{K}}}\sum_{nln'l'jj'}\langle n_q l_q n_{\mathcal{K}} l_{\mathcal{K}}:K|n'l'nl:K\rangle_{d=1}(-1)^{\frac{l-l'}{2}}(-1)^{j+\frac{1}{2}+l+l'+K}\hat{j}\hat{j}'\begin{Bmatrix} l' & l & K \\ j & j' & \frac{1}{2} \end{Bmatrix}$$
$$\times R_{n_q l_q}(q)R_{n_{\mathcal{K}} l_{\mathcal{K}}}(\mathcal{K})\langle A\lambda'J'||(a_{n'l'j'}^\dagger\tilde{a}_{nlj})^K||A\lambda J\rangle. \tag{23}$$

Next, we calculate the contribution of the c.m. as

$$\langle\phi_{\text{c.m.}}0s|e^{-i\vec{q}\cdot\vec{\zeta}_{\text{c.m.}}}|\phi_{\text{c.m.}}0s\rangle = e^{-\frac{1}{4A}b^2 q^2}, \tag{24}$$

where A is the number of nucleons and b the harmonic oscillator length. The explicit calculation is given in Appendix C.

Collecting the information from Eqs. (22) and (24), the ti nonlocal density can be calculated as

$$\rho(\vec{q},\vec{\mathcal{K}}) = e^{\frac{1}{4A}b^2 q^2}\rho_{sf}(\vec{q},\vec{\mathcal{K}}), \tag{25}$$

where we dropped the subscript ti. Since the c.m. contribution is a simple analytic function of q^2, the numerical effort in computing the ti nonlocal density is the computation of the sf nonlocal density as a function of $\vec{q}$ and $\vec{\mathcal{K}}$ in Eq. (21). This is an important advantage of the current method, and avoids the need for transforming NCSM's OBDM elements to relative (Jacobi) coordinates. Subsequently, we can obtain the ti nonlocal density in coordinate space by a Fourier transformation of Eq. (25). The ti local density can be computed from Eq. (25)

by integrating the nonlocal density over $\vec{\mathcal{K}}$,

$$\rho_{K=0}(q) = \int d\mathcal{K}\,\mathcal{K}^2\rho_{000}(q,\mathcal{K}). \tag{26}$$

Note that this local density in momentum space is also referred to as the elastic form factor (see, e.g., Ref. [31]), and can also be obtained as the Fourier transform of the local probability density in coordinate space. We use this as numerical check; in particular, the value at $q = 0$ should correspond to the number of nucleons.

III. RESULTS AND DISCUSSION

A. Nonlocal densities in momentum space

The nonlocal densities shown in this work are based on *ab initio* NCSM or SA-NCSM calculations of OBDM elements that employ the JISP16 *NN* interaction [25]. Before elaborating on the nonlocal structure of the translationally invariant

density, we first establish that its construction is consistent with
a translationally invariant local density directly constructed
in momentum space as outlined in Appendix A. In Fig. 1
we show the $K = 0$ component of the local proton density
of ^{12}C as a function of the momentum transfer q, which is
constructed as outlined in Appendix A. We also confirmed that
this is numerically equivalent to the local density construction
presented in Ref. [30]. The solid line represents the Fourier
transform of the density to momentum space, the form factor,
which is normalized at $q = 0$ to the number of protons.
The solid triangles represent the same quantity obtained by
integrating the nonlocal density over the nonlocal variable $\mathcal{K}$
according to Eq. (26). The integrated values agree with the
directly constructed ones at least within six significant figures.
For comparison, we also include a local density obtained
from a more traditional Hartree-Fock-Bogolyubov mean-field
calculation which utilizes the density-dependent finite-range
Gogny D1S nucleon-nucleon interaction [32,33]. Based on
this density, elastic proton scattering off ^{12}C was successfully
calculated in [34]. However, a slight mismatch in the diffraction
minima of the differential cross section could indicate that the
slower fall-off of the NCSM local density may be preferable.

Next, we want to study nonlocal one-body densities of four
different nuclei, the open shell nuclei ^{6}Li and ^{12}C, and the
closed shell nuclei ^{4}He and ^{16}O. It is well known that ^{12}C
consisting of six protons and six neutrons is deformed in its
body-fixed frame, ^{6}Li consisting of three protons and three
neutrons can be sometimes viewed as consisting of a ^{4}He core
and an additional neutron-proton pair in the p-shell, while ^{4}He
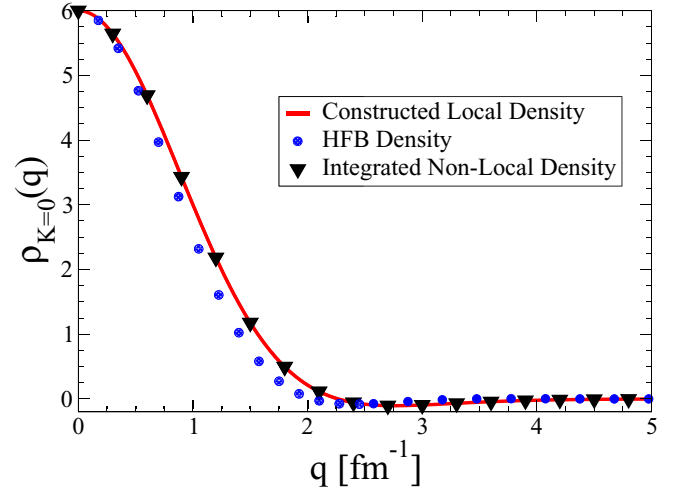and ^{16}O are closed shell nuclei. In a shell-model framework,

FIG. 1. The translationally invariant local one-body density obtained from a NCSM calculation ($N_{\max} = 10$, $\hbar\omega = 20$ MeV) based on the JISP16 *NN* interaction for the proton distribution of ^{12}C as function of the momentum transfer q. The solid line (red) shows the direct construction in momentum space, while the solid triangles (black) give the local density obtained by integrating the nonlocal density over the momentum $\mathcal{K}$. As comparison a local density obtained from a HFB mean field calculation based on the Gogny interaction [33] is shown by the filled solid (blue) circles.

the protons and neutrons in ^{4}He occupy predominantly the *s*
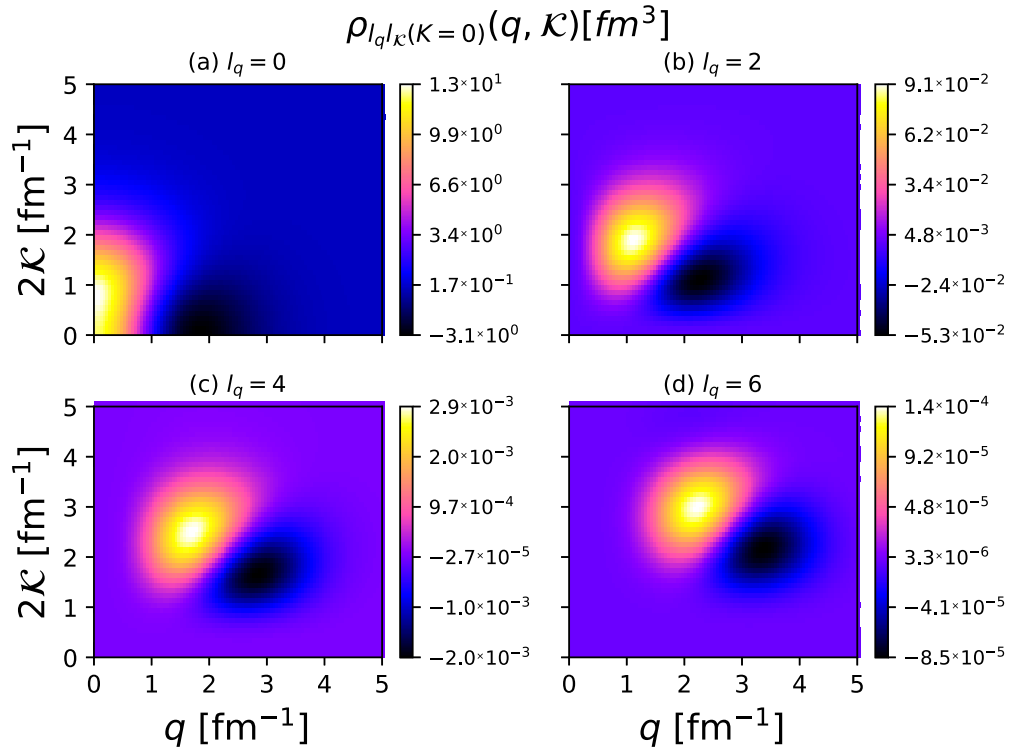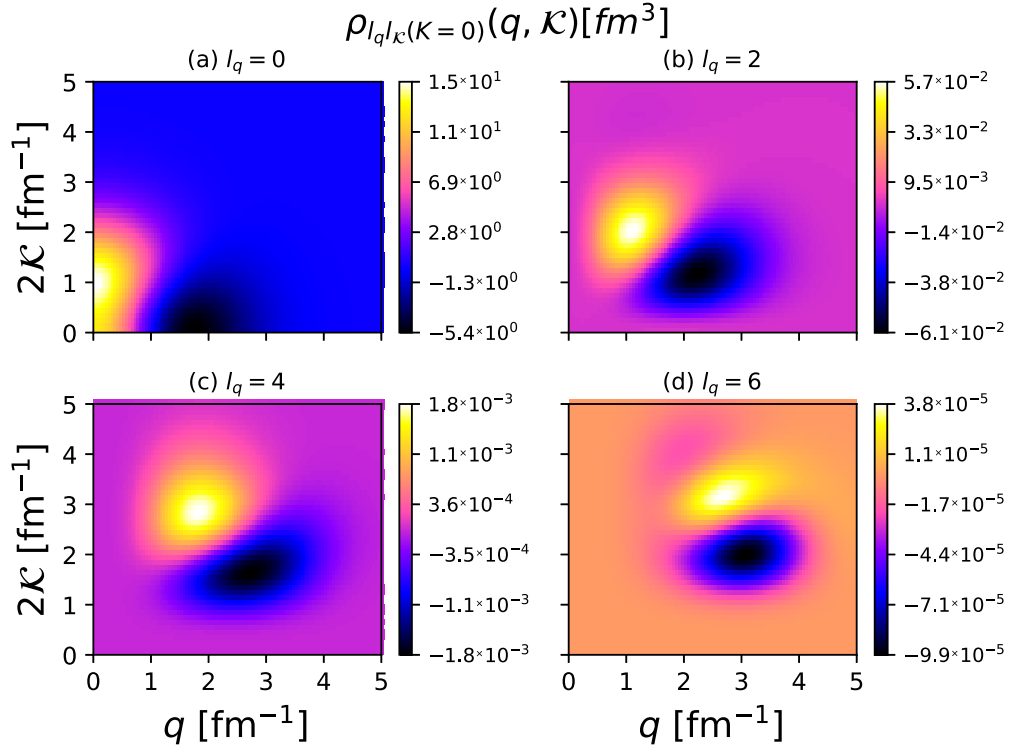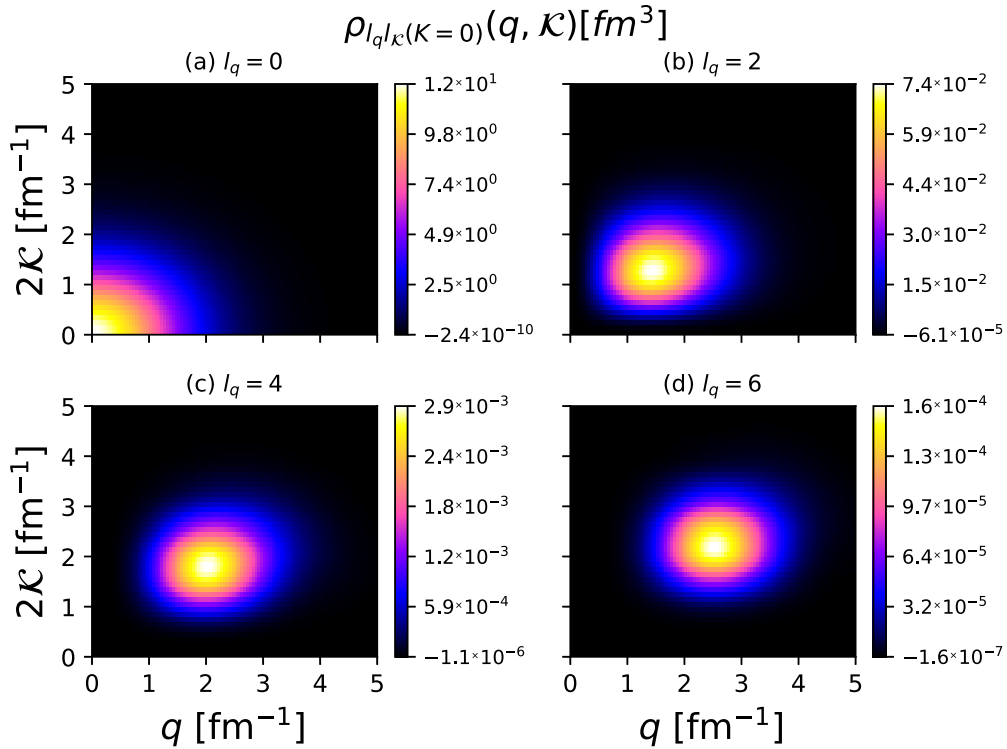shell, while in ^{16}O they occupy predominantly the *s* and *p*

FIG. 2. The $K = 0$ component of the translationally invariant nonlocal one-body density obtained from a NCSM calculation ($N_{\max} = 10$, $\hbar\omega = 20$ MeV) based on the JISP16 *NN* interaction for the proton distribution of ^{12}C as function of the momenta q and $\mathcal{K}$. Panel (a) depicts the contribution of $l_q = 0$, (b) of $l_q = 2$, (c) of $l_q = 4$, and (d) of $l_q = 6$.

$$\rho_{l_q l_{\mathcal{K}}(K=0)}(q, \mathcal{K})[fm^3]$$

FIG. 3. The $K = 0$ component of the translationally invariant nonlocal one-body density obtained from a NCSM calculation ($N_{max} = 8$, $\hbar\omega = 20$ MeV) based on the JISP16 *NN* interaction for the proton distribution of ^{16}O as function of the momenta q and $\mathcal{K}$. Panel (a) depicts the contribution of $l_q = 0$, (b) of $l_q = 2$, (c) of $l_q = 4$, and (d) of $l_q = 6$.

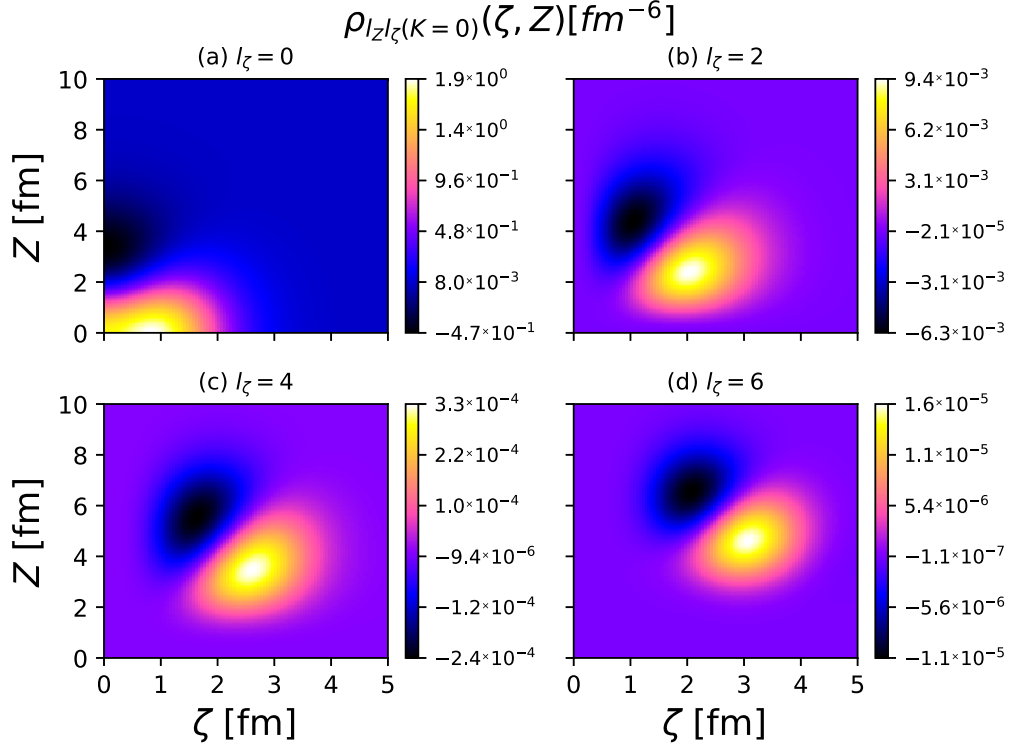$$\rho_{l_q l_{\mathcal{K}}(K=0)}(q, \mathcal{K})[fm^3]$$

FIG. 4. The $K = 0$ component of the translationally invariant nonlocal one-body density obtained from a NCSM calculation ($N_{max} = 14$, $\hbar\omega = 20$ MeV) based on the JISP16 *NN* interaction for the proton distribution of ^{4}He as function of the momenta q and $\mathcal{K}$. Panel (a) depicts the contribution of $l_q = 0$, (b) of $l_q = 2$, (c) of $l_q = 4$, and (d) of $l_q = 6$.
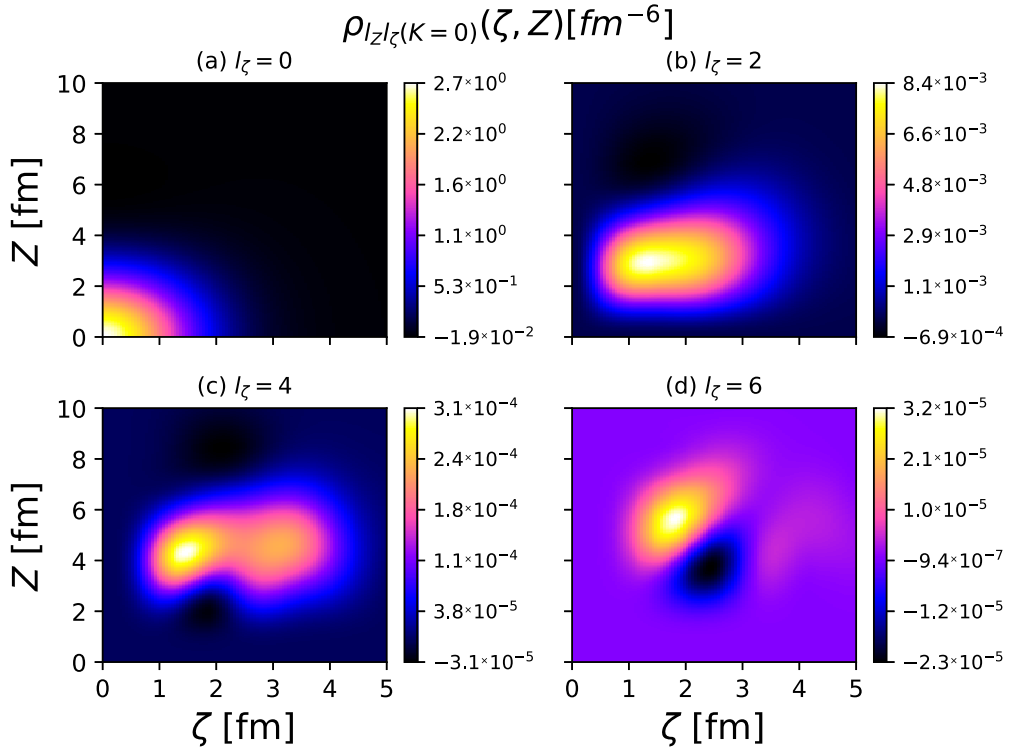
$$\rho_{l_Z l_\zeta (K=0)}(\zeta, Z)[fm^{-6}]$$

FIG. 5. The $K = 0$ component of the translationally invariant nonlocal one-body density obtained from a NCSM calculation ($N_{max} = 10, \hbar\omega = 20$ MeV) based on the JISP16 *NN* interaction for the proton distribution of ^{12}C as function of the local coordinate ζ and the nonlocal coordinate Z. Panel (a) depicts the contribution of $l_\zeta = 0$, (b) of $l_\zeta = 2$, (c) of $l_\zeta = 4$, and (d) of $l_\zeta = 6$.
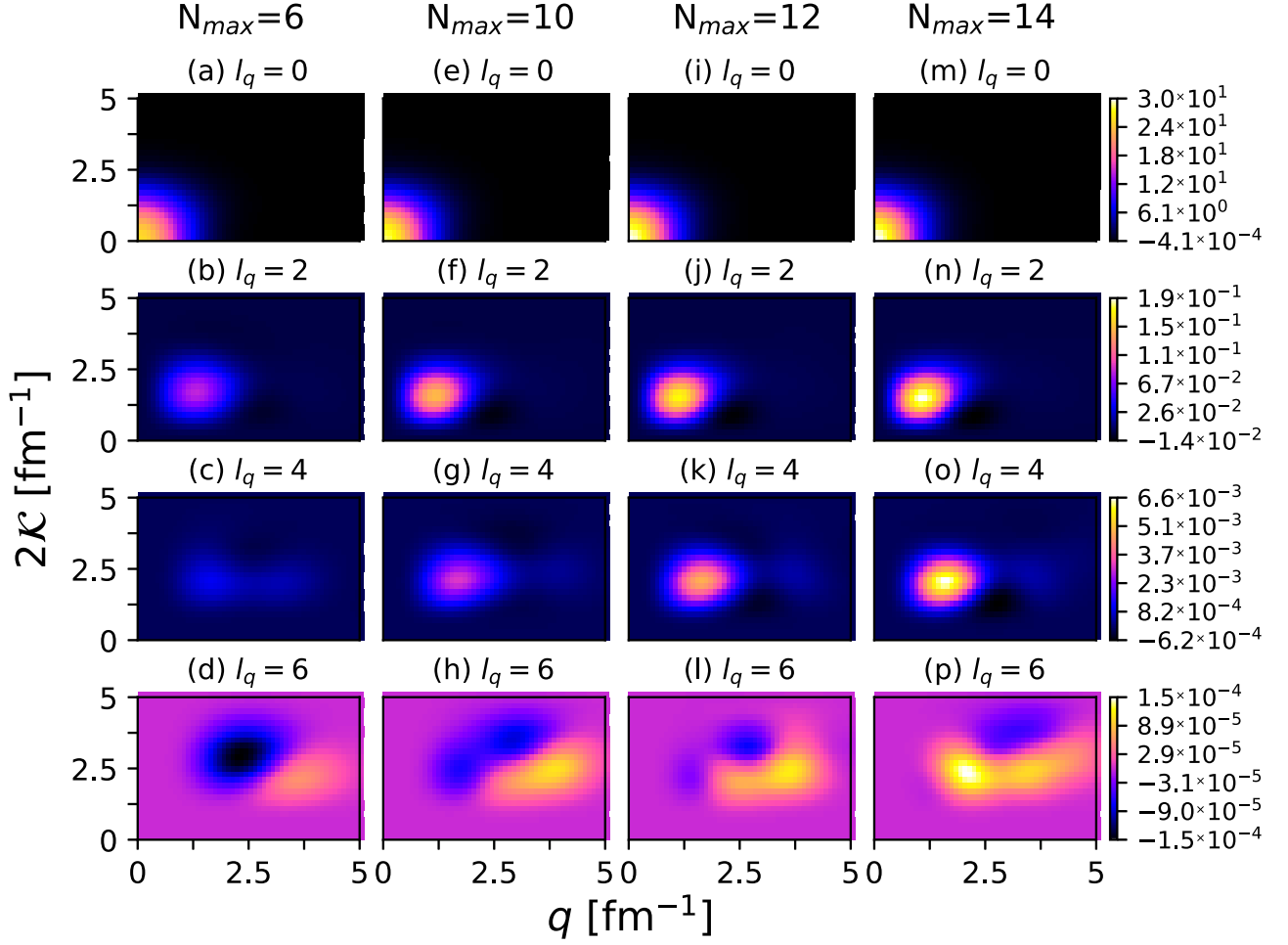
$$\rho_{l_Z l_\zeta (K=0)}(\zeta, Z)[fm^{-6}]$$

FIG. 6. The $K = 0$ component of the translationally invariant nonlocal one-body density obtained from a NCSM calculation ($N_{max} = 14, \hbar\omega = 20$ MeV) based on the JISP16 *NN* interaction for the proton distribution of ^{6}Li as function of the local coordinate ζ and the nonlocal coordinate Z. Panel (a) depicts the contribution of $l_\zeta = 0$, (b) of $l_\zeta = 2$, (c) of $l_\zeta = 4$, and (d) of $l_\zeta = 6$.

FIG. 7. The $K = 0$ component of the translationally invariant nonlocal one-body density $\rho_{l_q l_{\mathcal{K}}}(q,\mathcal{K})$ obtained from a NCSM calculation ($\hbar\omega = 20$ MeV) based on the JISP16 *NN* interaction for the proton distribution of ^{6}Li as function of the momenta q and $\mathcal{K}$ and the size of the model space. The first column contains angular momentum slices obtained with $N_{\max} = 6$, the second with $N_{\max} = 10$, the third with $N_{\max} = 12$, and the fourth with $N_{\max} = 14$. The rows represent different angular momentum slices $l_q = l_{\mathcal{K}}$ from 0 to 6.

shells. Thus we want to explore if nonlocal properties reflect some of the common perceptions about those nuclei. Since we make a multipole expansion of the nonlocal density, it is convenient to concentrate on a specific multipole. Here we chose the $K = 0$ multipole, since this component determines the density of the 0^+ ground states for the even-even nuclei under consideration and dominates in the 1^+ ground state in ^{6}Li. First, we want to consider the $K = 0$ multipole [see Eq. (23) for notation] of the nonlocal one-body density in momentum space, $\rho_{l_q l_{\mathcal{K}}(K=0)}(q,\mathcal{K})$. We show proton densities in physically relevant variables, the momentum transfer $q = |\vec{p}' - \vec{p}|$ and $\mathcal{K} = \frac{1}{2}|\vec{p}' + \vec{p}|$. Note that the variable $\vec{\mathcal{K}}$, being the conjugate coordinate to the nonlocal coordinate $\vec{Z}$, only appears when nonlocal densities are considered. The converged nonlocal densities $\rho_{l_q l_{\mathcal{K}}(K=0)}(q,\mathcal{K})$ for the proton distributions of ^{12}C, ^{16}O, and ^{4}He are displayed as functions of q and $\mathcal{K}$ in Figs. 2, 3, and 4, respectively, while the corresponding nonlocal density of ^{6}Li is given in the last column of Fig. 7. To illustrate the contributions of different angular momenta, we show slices of constant values of $l_q = l_{\mathcal{K}}$. The constraints given in Eq. (21) indicate that, for $K = 0$, once l_q is fixed, $l_{\mathcal{K}}$ takes the same value.

We also need to point out that the contributions of odd values of l_q cancel out exactly for $K = 0$ as a result of the symmetry properties of the Talmi-Moshinsky brackets [35,36]. The vanishing contribution for odd l_q is validated numerically as well.

A common observations for all four nuclei is that the contribution of $l_q = 0$ dominates. We further point out that, when integrating $\rho_{l_q l_{\mathcal{K}}(K=0)}(q,\mathcal{K})$ over $\mathcal{K}$ to obtain the local density, the constraints for l_q determine that only $l_q = 0$ contributes to the local density, as given, e.g., for ^{12}C in Fig. 1. Thus, all higher values of l_q are genuinely nonlocal contributions for $K = 0$. For both ^{6}Li and ^{4}He, the maximum of the $l_q = 0$ slice is located at $q = 0$ and $\mathcal{K} = 0$, and the functions fall off smoothly to zero in q as well $\mathcal{K}$. This is different for ^{12}C and ^{16}O, for which the maximum value is located around $\mathcal{K} \sim 1$ fm^{-1} and $q = 0$, and which, in addition, exhibit a minimum around $q \sim 2$ fm^{-1} for $\mathcal{K} = 0$.

Figures 2–4 as well as Figs. 7–9 are plotted in a way that $\rho_{l_q l_{\mathcal{K}}}(q = 2\mathcal{K},\mathcal{K})$ is shown along the diagonal. For the closed shell nucleus ^{4}He (Fig. 4), for which the protons are assumed to dominantly occupy the s shell, the maximum of the nonlocality for $l_q \geqslant 2$ follows the diagonal line and moves to higher values

of q the larger l_q becomes. For ^{6}Li (Fig. 7, fourth column), which can still be considered as dominated by particles in the s shell, the maximum of $\rho_{l_q l_{\mathcal{K}}}(q, \mathcal{K})$ moves slightly away from the "diagonal" and the off-shell structure can be roughly located between $\rho_{l_q l_{\mathcal{K}}}(q = 4\mathcal{K}, \mathcal{K})$ and $\rho_{l_q l_{\mathcal{K}}}(q = \mathcal{K}, \mathcal{K})$, while for ^{12}C (Fig. 2) and ^{16}O (Fig. 3) the entire nonlocality is located in this "wedge." Furthermore the density changes sign along the line $q = 2\mathcal{K}$. This pattern, together with the different $l_q = 0$ behavior, appears to be a signature for nonlocal densities in p-shell dominated nuclei.

B. Nonlocal densities in coordinate space

Once we obtain the *ti* nonlocal density in momentum space, we can numerically Fourier transform them to coordinate space. The conjugate coordinate to the momentum transfer q is the local coordinate $\zeta = \frac{1}{2}|\vec{r}' + \vec{r}|$, and to $\mathcal{K}$ the nonlocal coordinate $Z = |\vec{r}' - \vec{r}|$. The angular momenta related to ζ and Z are denoted as l_ζ and l_Z. In Fig. 5 we show angular momentum slices of nonlocal proton densities in coordinate space for $K = 0$ as a function of ζ and Z for ^{12}C, and in Fig. 6 for ^{6}Li. Here we choose the local coordinate ζ as one

of the axes, so that one can directly read off the local densities of ^{12}C and ^{6}Li along the line $Z = 0$. Hence, Fig. 5 shows that the local density of ^{12}C has its maximum at $\zeta \sim 1$ fm and is suppressed at $\zeta = 0$ fm, suggesting that the density is pushed away from the center; indeed, if one plots this density in a body-fixed frame, it will have a deformed torus-like shape with a suppressed density in the center. However, the present densities are not calculated in a body-fixed frame, and Fig. 5 does not reveal any features that can be associated with the nuclear deformation. On the other hand, we can say that when we compare the $l_q = 0$ contributions in momentum space of ^{12}C and ^{16}O, the local density of ^{16}O also has a maximum that is pushed away from the origin, which is a consequence of the p shell being filled up.

The range of the ζ and Z axes are chosen such that the diagonal of the plot shows $\rho_{l_\zeta l_Z}(\zeta, Z = 2\zeta)$. Both figures show similar behavior for $l_\zeta \geqslant 2$ as the corresponding q-$\mathcal{K}$ figure. In Fig. 5 for $l_\zeta \geqslant 2$, the nonlocal density changes sign along $\rho_{l_\zeta l_Z}(\zeta, Z = 2\zeta)$, and the maxima and minima are roughly located in the area given by the lines $\zeta = 4Z$ and $\zeta = Z$, indicating a possible p-shell dominance of the nonlocal density. For ^{6}Li the situation is slightly different: for $l_\zeta = 2$ the

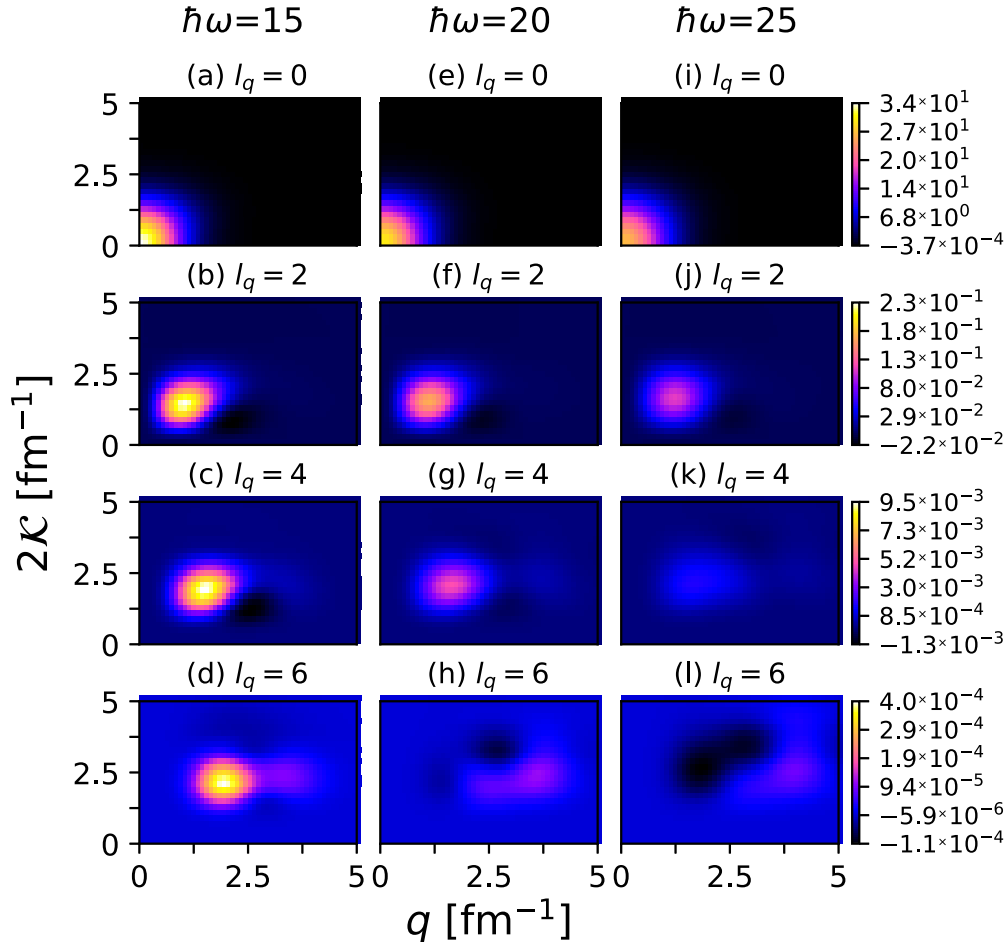FIG. 8. The $K = 0$ component of the translationally invariant nonlocal one-body density $\rho_{l_q l_{\mathcal{K}}}(q, \mathcal{K})$ obtained from a NCSM calculation ($N_{\max} = 12$) based on the JISP16 *NN* interaction for the proton distribution of ^{6}Li as function of the momenta q and $\mathcal{K}$ and the oscillator parameter $\hbar\omega$. The first column contains angular momentum slices obtained with $\hbar\omega = 15$ MeV, the second with $\hbar\omega = 20$ MeV, and the third with $\hbar\omega = 25$ MeV. The rows represent different angular momentum slices $l_q = l_{\mathcal{K}}$ from 0 to 6.

maximum still follows the diagonal, and only for $l_\zeta \geqslant 4$ does a p-shell dominance develop. This may indicate that the lower l_ζ are still s-shell dominated, while the p-shell proton mainly gives the $l_\zeta = 6$ contribution.

A further study of NCSM calculations with different NN interactions will have to be carried out to investigate if the observed nonlocal structures persist and are essentially an indication of the shell structure of the nucleus under consideration.

C. Dependence of the nonlocal density on the model space

The calculations presented in the previous subsections are carried out with one-body density matrix elements from NCSM and SA-NCSM calculations that are close to convergence with respect to the ground state binding energies and low-lying excited states, as far as the model space is concerned. For ^{6}Li those studies are carried out in Ref. [30,31,37], together with model-dependence studies with respect to the root-mean-square point-proton radius and the quadrupole moment. The calculations for ^{12}C are discussed in Ref. [37] and those for ^{16}O in Refs. [38,39]. The ti density should become independent of

the basis parameters $\hbar\omega$ and $N_{\max}$ as $N_{\max}$ increases. However, it is impractical to carry out a convergence study of the nonlocal density itself, and instead we illustrate how some of the features of the nonlocal density depend on the model space.

First, we consider the $K = 0$ component of the nonlocal proton density for a fixed $\hbar\omega = 20$ MeV as a function of the $N_{\max}$ truncation. In Fig. 7 we display slices of $\rho_{l_q l_K}(q, \mathcal{K})$ for ^{6}Li for fixed $l_q = l_{\mathcal{K}}$ for $N_{\max} = 6$, 10, 12, and 14. For $l_q = 0$ we observe that the density maximum at $q = 0$, $\mathcal{K} = 0$ increases as a function of $N_{\max}$. This is consistent with the fact that the tail of the wave function in coordinate space (and hence radii) become better described as $N_{\max}$ increases. However, the general distribution remains the same. The angular momentum slices $l_q = 2$ and $l_q = 4$ clearly show how the nonlocal structure builds up as $N_{\max}$ increases, but again the general distribution remains the same. Even going from $N_{\max} = 12$ to $N_{\max} = 14$, there is a very slight increase of the maxima of $\rho_{l_q l_K}$. The slice for $l_q = 6$ for $N_{\max} = 6$ exhibits a very different nonlocal structure in comparison to the higher $N_{\max}$ values, which can be understood as an effect of the model-space truncation. We observe changes in the nonlocal
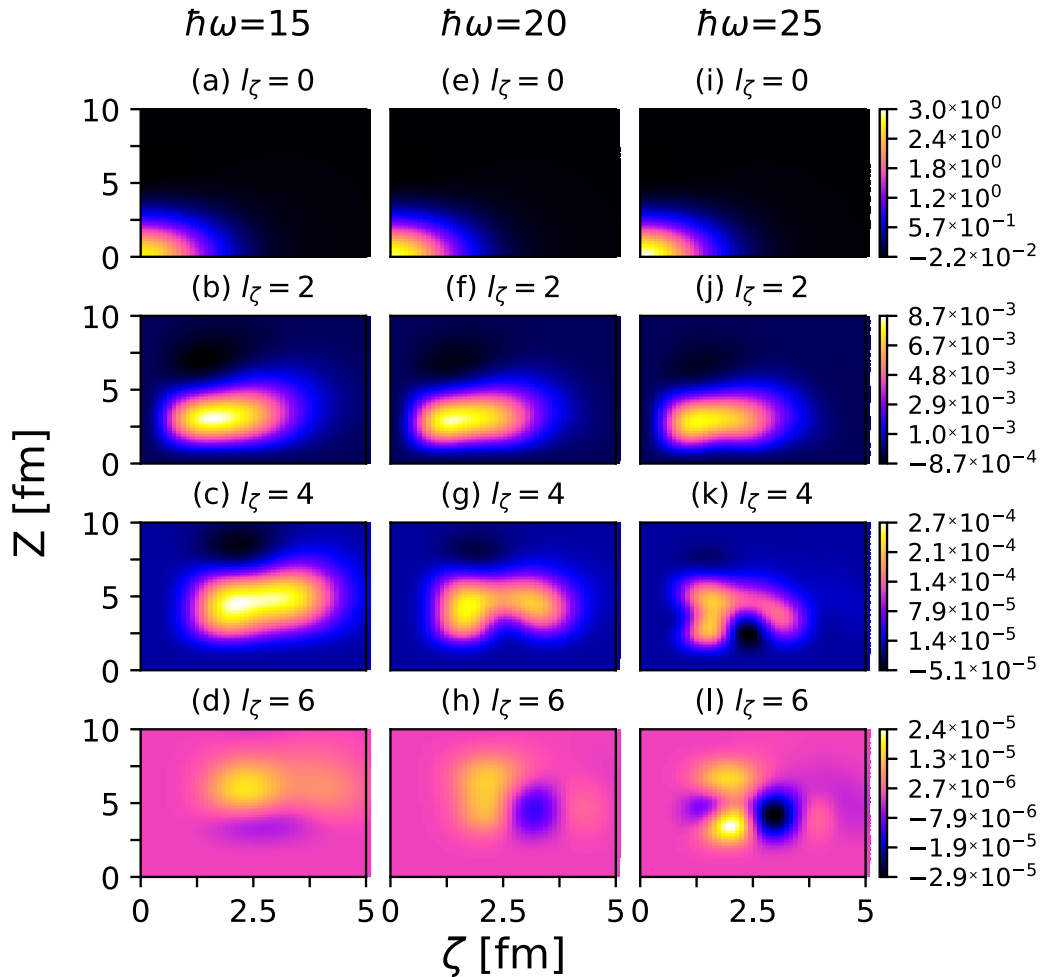

FIG. 9. The $K = 0$ component of the translationally invariant nonlocal one-body density $\rho_{l_\zeta l_Z}(\zeta, Z)$ obtained from a NCSM calculation ($N_{\max} = 12$) based on the JISP16 NN interaction for the proton distribution of ^{6}Li as function of the local coordinate ζ, the nonlocal coordinate Z, and the oscillator parameter $\hbar\omega$. The first column contains angular momentum slices obtained with $\hbar\omega = 15$ MeV, the second with $\hbar\omega = 20$ MeV, and the third with $\hbar\omega = 25$ MeV. The rows represent different angular momentum slices $l_\zeta = l_Z$ from 0 to 6.

structure for $l_q = 6$ even when going from $N_{max} = 12$ to $N_{max} = 14$. However, the absolute values of this contribution is so small that calculations of observables based on this nonlocal density are unlikely to be affected by the $l_q = 6$ (or higher) contributions. In general, the figure shows that the $N_{max} = 6$ model space is not sufficient to describe nonlocal correlations, but the nonlocal structure looks reasonably well converged at $N_{max} = 14$, similarly to the results calculated earlier for the binding energy and other observables [30].

Next we keep N_{max} fixed ($N_{max} = 12$) and study the nonlocal structure as a function of the oscillator parameter $\hbar\omega$, where we choose the values 15, 20, and 25 MeV. It is well known that, for a given N_{max}, the basis truncation introduces effective infrared (IR) cutoff and ultraviolet (UV) cutoffs that also depend on the $\hbar\omega$ value: namely, very low $\hbar\omega$ values (a small momentum UV cutoff) cut out high momenta that may affect short-range correlations, while very large $\hbar\omega$ values (small spatial IR cutoff) affect the wave function tail [40–43]. Note that increasing N_{max} increases both the IR and UV cutoffs, removing both cutoffs in the infinite model space limit. Exploring the $\hbar\omega$ dependence, in comparison to the large N_{max} limit of Fig. 7 which improves both cutoffs, can provide some indication if the nonlocality is sensitive to these cutoffs. The corresponding functions $\rho_{l_q l_{\mathcal{K}}}(q, \mathcal{K})$ for $l_q = l_{\mathcal{K}} = 0, 2, 4$, and 6 are shown in Fig. 8 and $\rho_{l_\zeta l_Z}(\zeta, Z)$ in Fig. 9 for the proton density of ^{6}Li. The study of Ref. [30] has already shown that, for the local density $\rho(r)$ of ^{6}Li, a smaller value of $\hbar\omega$ leads to a better description of the asymptotic tail of the wave function and a spatially expanded density, but the density in the nucleus interior becomes low, whereas for larger values of $\hbar\omega$ the situation is reversed. Indeed, the larger $\hbar\omega$ value yields a significantly lower maxima for the density in momentum space (Fig. 8), whereas the smaller $\hbar\omega$ value gives very pronounced maxima as function of q and $\mathcal{K}$. As already mentioned above, this is the result of the poor convergence of the tail of the wave function in coordinate space for large values of $\hbar\omega$. On the other hand, low $\hbar\omega$ values lack a good description of the high momentum behavior. Furthermore, for low $\hbar\omega$ the maxima are moved toward low q momentum transfers, and for high l_q a particle is mainly transferred from (or to) low p momentum (diagonal line, as discussed above).

Considering the coordinate space density, $\rho_{l_\zeta l_Z}(\zeta, Z)$, in Fig. 9, we find that for small $\hbar\omega$ values, the nonlocal structures are well developed at larger values of ζ and l_ζ, while for $l_\zeta = 0$ the maximum at $\zeta = Z = 0$ is less developed. Again, this is consistent with the findings in Ref. [30]. In contrast, for $\hbar\omega = 25$ MeV, we notice that more features are resolved in the nonlocal structure, especially for higher l_ζ, a direct result of improving the UV cutoff. Overall, we conclude that the nonlocality of the density seems to be more sensitive to the IR cutoff, that is, to the description of the tail of the wave function in coordinate space, except for high l_q, where the nonlocal contribution, while being very small, becomes also sensitive to the UV cutoff.

D. Study of the nonlocality of the density

To study the nonlocal behavior in a more quantitative fashion, we plot the $K = 0$, $l_q = 0$ component of $\rho_{l_q l_{\mathcal{K}}}(q, \mathcal{K})$
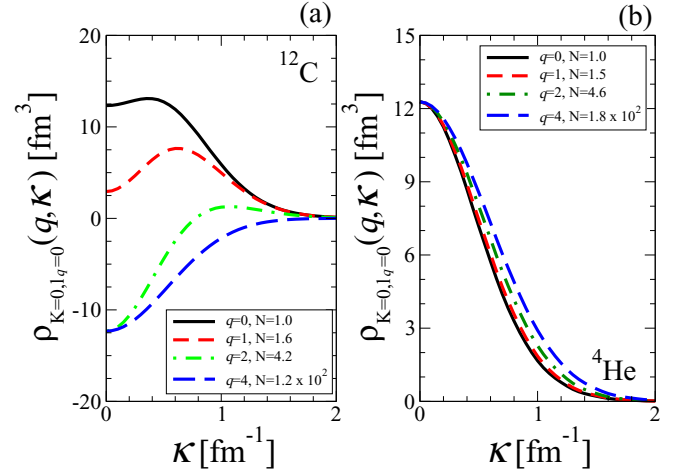

FIG. 10. The $K = 0$, $l_q = 0$ component of the translationally invariant nonlocal one-body density obtained from a NCSM calculation based on the JISP16 *NN* interaction for the proton distribution of ^{12}C [panel (a)] and ^{4}He (panel (b)) as a function of the nonlocal momentum $\mathcal{K}$ at fixed momenta q as indicated in the legend. The distributions are normalized by the factors indicated in the legend.

for fixed values of q as a function of $\mathcal{K}$ for ^{12}C [Fig. 10(a)] and ^{4}He [Fig. 10(b)]. As soon as we take $\mathcal{K}$-slices of ^{12}C at higher values of q, the form of the nonlocality changes, dips for $q = 1$ fm^{-1} for small $\mathcal{K}$, and becomes negative for even larger q. Since the magnitude of $\rho_{K=0,l_q=0}(q, \mathcal{K})$ changes by orders of magnitude when moving along q, we normalize the slices by a factor N given by

$$N = \frac{\rho(q = 0, \mathcal{K} = 0)}{\rho(q, \mathcal{K} = 0)}. \quad (27)$$

We also note that $\rho_{K=0,l_q=0}(q, \mathcal{K})$ falls off quickly as a function of $\mathcal{K}$, independent of the value of q, and becomes essentially zero for $\mathcal{K} \geqslant 2$ fm^{-1}. Comparing with Fig. 3, the nonlocal density of ^{16}O exhibits the same behavior. Panel (b) of Fig. 10 shows similar slices of the $K = 0$ component of $\rho_{l_q l_{\mathcal{K}}}(q, \mathcal{K})$ for ^{4}He. Here we find that the nonlocal density is positive for all values of q and falls off like a Gaussian. However, there is no uniform Gaussian bell shape for all q, since for the larger q values the Gaussian width increases. It appears that there is no simple parametrization of this behavior as a function of q. Similarly to ^{12}C, the nonlocality of the ^{4}He density is essentially zero for $\mathcal{K} > 2$ fm^{-1}, though it has larger high-momentum components compared to ^{12}C. This can be understood from realizing that smaller radii in coordinate space translate to larger high-momentum components.

Finally, we show in Fig. 11(a) a "form factor" $\rho_{K=0}(\mathcal{K})$, for $K = 0$, as a function of $\mathcal{K}$, where $\rho_{l_q l_{\mathcal{K}}}(q, \mathcal{K})$ is integrated over q. It is worthwhile noting that for ^{4}He and ^{6}Li this function is positive, while it starts as negative values for ^{12}C and ^{16}O before turning positive. This, together with the observations of Sec. III A, may allow one to conclude that if a nucleus is dominated by s-shell nucleons, the value of $\rho_{K=0}(\mathcal{K} = 0)$ is positive, and when p-shell nucleons dominate, $\rho_{K=0}(\mathcal{K} = 0)$ is negative.
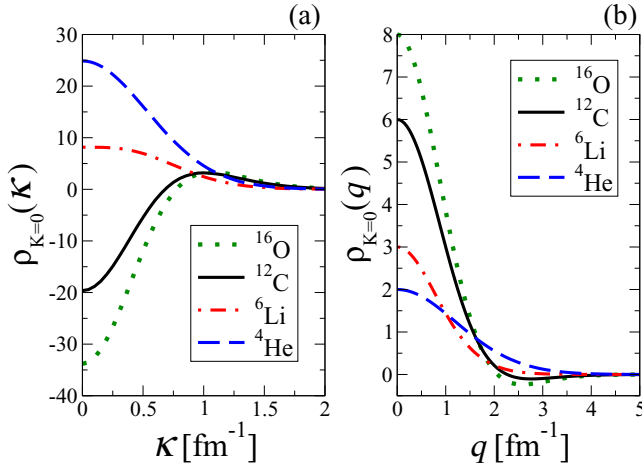
FIG. 11. The $K = 0$ component of the translationally invariant one-body density obtained from NCSM calculations based on the JISP16 *NN* interaction for the proton distributions of ^{4}He, ^{6}Li, ^{12}C, and ^{16}O as a function of the nonlocal momentum $\mathcal{K}$ when integrated of the local momentum q [panel (a)]. Panel (b) depicts the local densities for the same nuclei as function of the momentum transfer q when integrated over the nonlocal momentum $\mathcal{K}$.

In addition, we show in Fig. 11(b) the conventional proton form factors (local densities in momentum space) for the same nuclei, which are normalized to the proton number at $q = 0$. Only the charge distributions of the heavier nuclei have a zero crossing visible in the figure; the one for ^{6}Li turns negative at ∼6 fm^{-1} while it stays completely positive for ^{4}He. Generally, the proton form factor provides information about the spatial charge distribution of the nucleus. The information given by $\rho_{K=0}(\mathcal{K})$ gives a consistent picture; namely, after the *s*-shell is filled, additional protons fill up the *p* shell.

IV. CONCLUSIONS AND OUTLOOK

In this work we explored features of translationally invariant nonlocal one-body densities obtained from *ab initio* NCSM and SA-NCSM calculations using the JISP16 *NN* interaction [25] for several light nuclei. In order to do this, we first defined the nonlocal one-body density in a space-fixed coordinate system in such a way that it directly relates to the OBDM elements which a NSCM calculation provides, and constructed space-fixed nonlocal one-body densities for ^{4}He, ^{6}Li, ^{12}C, and ^{16}O in momentum and position space. As examples for our study, we chose ^{4}He and ^{16}O representing closed shell nuclei, together with ^{6}Li and ^{12}C representing open shell nuclei.

To remove the c.m. part of the wave functions calculated in the NCSM using a harmonic oscillator basis, we first needed to transform the space-fixed nonlocal densities from conventionally used linearly independent variables $\vec{p}$ and $\vec{p}'$ to another linearly independent set $\vec{q}$ and $\vec{\mathcal{K}}$ which is more appropriate for our task. Their conjugate coordinate variables $\vec{\zeta}$ and $\vec{Z}$ are such that the c.m. contribution is only contained in $\vec{\zeta}$. With this, we can successfully extend a scheme developed

for removing c.m. contributions from local one-body densities [27–31] to nonlocal one-body densities.

We studied the nonlocal structure of the one-body densities as a function of the angular momentum l_q in momentum as well as coordinate space. For all four nuclei the largest contribution to the nonlocal density comes from the $l_q = 0$ part, for which the nonlocality is restricted to about 2 fm. The higher angular momenta, though at least two orders of magnitude smaller, contribute exclusively to the nonlocal structure. Thus nuclear properties or reactions that are dominated by these angular momentum contributions will show sensitivity to the nonlocality. In addition, we found that the nonlocal structure of the neutron and proton one-body densities does not show any significant difference for the $N = Z$ nuclei we investigated. We also found that the structure of the nonlocality reflects the shell structure of the nuclei we considered. Once the *p* shell becomes dominant, the nonlocality exhibits a specific pattern not visible in the *s*-shell dominated ^{4}He. Finally, we investigated if there may be some systematic behavior in the nonlocal structure of the one-body densities which might be captured in some analytic form. While this might be possible for the nonlocal structure of ^{4}He, it does not look promising for the other nuclei we investigated.

We note that the current results are presented for the JISP16 *NN* interaction, and we have found that, e.g., using chiral potentials such as the NNLO$_{\text{opt}}$ [44] for ^{6}Li does not introduce significant changes into the density outcomes presented here. A further study that adopts different *NN* interactions will have to be carried out to investigate if the observed nonlocal structures persist and are essentially an indication of the nuclear shell structure. We have also studied the role of nonlocality in densities calculated from the SA-NCSM using selected model spaces, which yields results that are essentially the same as compared to those obtained in the corresponding complete model spaces. This will allow one to study nonlocal density features in heavier nuclear systems. The outcomes of these studies will be the focus of a following publication.

Summarizing, this work shows how the c.m. contribution can be removed from *ab initio* nonlocal one-body densities using NCSM wave functions, in a way similar to that known for local ones. This will open the path for those densities to be employed, for example, in calculations of nuclear reactions.

APPENDIX A: DERIVATION OF THE SPACE-FIXED LOCAL ONE-BODY DENSITY CONSTRUCTED IN MOMENTUM SPACE

To apply the procedure for removing the c.m. contribution from the local density as suggested in Refs. [30,31,43], the space-fixed local density constructed in coordinate space needs to be Fourier transformed to momentum space. A numerical Fourier transform as suggested in [30] will introduce numerical errors specifically at large momenta due to the highly oscillatory nature of the transformation. Therefore, it is highly desirable to derive a scheme in which the space-fixed local density is constructed directly in momentum space. For this, we need the HO wave functions, $R_{nl}(p)$, in momentum space:

$$R_{nl}(p) = (-1)^n \left[\frac{2(b^2)^{l+3/2}\Gamma(n+1)}{\Gamma(n+l+\frac{3}{2})} \right]^{\frac{1}{2}} p^l e^{-\frac{1}{2}p^2 b^2} L_n^{l+\frac{1}{2}}(p^2 b^2), \tag{A1}$$

with harmonic oscillator length $b = \sqrt{\frac{\hbar^2 c^2}{mc^2\hbar\Omega}}$. The corresponding coordinate space HO wave functions are given as

$$R_{nl}(r) = \sqrt{\frac{2}{\pi}} \int dp \, p^2 R_{nl}(p) j_l(rp) = \left[\frac{2\Gamma(n+1)}{(b^2)^{l+\frac{1}{2}}\Gamma\left(n+l+\frac{3}{2}\right)} \right]^{\frac{1}{2}} r^l e^{-\frac{1}{2}\frac{r^2}{b^2}} L_n^{l+\frac{1}{2}}\left(\frac{r^2}{b^2}\right). \tag{A2}$$

Here a normalization coefficient $\sqrt{\frac{2}{\pi}}$ is included. The function $L_n^{l+\frac{1}{2}}(\frac{r^2}{b^2})$ represents the associated Laguerre polynomials. Note the difference in phase of $(-1)^n$ in $R_{nl}(p)$ and $R_{nl}(r)$.

Combining this with the multipole expansion of the space-fixed nonlocal one-body density in Eqs. (6) and (7), we arrive at

$$\rho_{sf}^{(K)}(\vec{r},\vec{r}') = \sum_{nljn'l'j'} \sum_{K=|l-l'|}^{l+l'} (-1)^{J'-M'} \begin{pmatrix} J' & K & J \\ -M' & 0 & M \end{pmatrix} \sum_{m,m'} \langle lml'm'|K0\rangle Y_l^{*m}(\hat{r}) Y_{l'}^{*m'}(\hat{r}')$$

$$\times \hat{j}\hat{j}'(-1)^{l'+l+j+\frac{1}{2}+K} \begin{Bmatrix} l' & l & K \\ j & j' & \frac{1}{2} \end{Bmatrix} \sqrt{\frac{2}{\pi}} \int dp \, p^2 R_{nl}(p) j_l(rp) \sqrt{\frac{2}{\pi}} \int dp' \, p'^2 R_{n'l'}(p') j_l(r'p')$$

$$\times \langle A\lambda' J' || (a_{n'l'j'}^\dagger \tilde{a}_{nlj})^{(K)} || A\lambda J \rangle. \tag{A3}$$

Setting $\vec{r} = \vec{r}'$, reducing the spherical harmonics, and simplifying the resulting Clebsch-Gordan coefficients by combining them with the $6j$ symbol leads to

$$\rho_{sf}^{(K)}(\vec{r}) = \sum_{nljn'l'j'} \sum_{K=|l-l'|}^{l+l'} (-1)^{J'-M'} \begin{pmatrix} J' & K & J \\ -M' & 0 & M \end{pmatrix} \begin{pmatrix} j' & j & K \\ \frac{1}{2} & -\frac{1}{2} & 0 \end{pmatrix} \frac{1}{\sqrt{4\pi}} \hat{j}\hat{j}'(-1)^{j+\frac{3}{2}+K} Y_K^{*0}(\hat{r})$$

$$\times \sqrt{\frac{2}{\pi}} \int dp\,p^2 R_{nl}(p) j_l(rp) \sqrt{\frac{2}{\pi}} \int dp'\,p'^2 R_{n'l'}(p') j_l(rp') \langle A\lambda' J' || (a_{n'l'j'}^\dagger \tilde{a}_{nlj})^{(K)} || A\lambda J \rangle. \tag{A4}$$

Rearranging the integrals and performing the Fourier transformation leads to

$$\rho_{sf}^{(K)}(\vec{q}) = \sum_{nljn'l'j'} \sum_{K=|l-l'|}^{l+l'} (-1)^{J'-M'} \begin{pmatrix} J' & K & J \\ -M' & 0 & M \end{pmatrix} \begin{pmatrix} j' & j & K \\ \frac{1}{2} & -\frac{1}{2} & 0 \end{pmatrix} \frac{1}{\sqrt{4\pi}} \hat{j}\hat{j}'(-1)^{j+\frac{3}{2}+K} (i)^K$$

$$\times Y_K^{*0}(\hat{r}) \langle A\lambda' J' || (a_{n'l'j'}^\dagger \tilde{a}_{nlj})^{(K)} || A\lambda J \rangle 8 \int dp\,p^2 R_{nl}(p) \int dp'\,p'^2 R_{n'l'}(p') \int dr\,r^2 j_K(qr) j_l(rp) j_{l'}(r'p'). \tag{A5}$$

For the special case of $K = 0$, the integral over r can be evaluated analytically, noting that $l = l'$ and $j = j'$:

$$\int dr\,r^2 j_0(qr) j_l(rp) j_{l'}(rp') = \frac{\pi}{4} \frac{\beta(\Delta)}{pp'q} P_l(\Delta). \tag{A6}$$

Here $P_l(\Delta)$ are Legendre polynomials, and the argument Δ is defined as

$$\Delta = \frac{p^2 + p'^2 - q^2}{2pp'}. \tag{A7}$$

The function $\beta(\Delta)$ is given as

$$\begin{aligned}
\beta(\Delta) &= 1 && \text{for } -1 < \Delta < 1, \\
\beta(\Delta) &= 1/2 && \text{for } \Delta = \pm 1, \\
\beta(\Delta) &= 0 && \text{otherwise.}
\end{aligned} \tag{A8}$$

The function $\beta(\Delta)$ allows us to constrain the integral over p' in Eq. (A4) to the values

$$p' \leqslant q + p \quad \text{and} \quad p' \geqslant |q - p|. \tag{A9}$$

This leads to the final expression for the momentum space local density, which can be calculated directly in momentum space from given OBDM elements from NCSM calculations:

$$\begin{aligned}
\rho_{sf}^{(0)}(q) = \sum_{nn'lj} (-1)^{J'-M'} &\begin{pmatrix} J' & 0 & J \\ -M' & 0 & M \end{pmatrix} \begin{pmatrix} j & j & 0 \\ \frac{1}{2} & -\frac{1}{2} & 0 \end{pmatrix} \\
&\times \sqrt{\pi} \, \hat{j} \hat{j} (-1)^{j+\frac{3}{2}} Y_0^{*0}(\hat{r}) \langle A\lambda' J' || (a_{n'lj}^\dagger \tilde{a}_{nlj})^{(0)} || A\lambda J \rangle \\
&\times \int_0^\infty dp \, p^2 R_{nl}(p) \int_{|p-q|}^{p+q} dp' \, p'^2 R_{n'l}(p') \frac{1}{pp'q} P_l(\Delta).
\end{aligned} \tag{A10}$$

APPENDIX B: DERIVATION OF HARMONIC OSCILLATOR LENGTHS FOR THE TRANSFORMATION TO q AND $\mathcal{K}$

For transforming the momenta of $\rho(\vec{p}, \vec{p}')$ in Eq. (11) to momenta $\vec{q}$ and $\vec{\mathcal{K}}$ we need to know how the harmonic oscillator lengths transform. Defining $b_\mathcal{K}$ and b_q, we can infer that a dimensionless coordinate transformation must hold in the same fashion as the coordinate transformation defined

in Eq. (14),

$$\begin{aligned}
b_\mathcal{K} \vec{\mathcal{K}} &= \frac{b_\mathcal{K}}{2b} b\vec{p}' + \frac{b_\mathcal{K}}{2b} b\vec{p}, \\
b_q \vec{q} &= \frac{b_q}{b} b\vec{p}' - \frac{b_q}{b} b\vec{p}.
\end{aligned} \tag{B1}$$

The transformation can be written as

$$\begin{pmatrix} b_\mathcal{K} \vec{\mathcal{K}} \\ b_q \vec{q} \end{pmatrix} = \begin{bmatrix} \sqrt{\frac{d}{1+d}} & \sqrt{\frac{1}{1+d}} \\ \sqrt{\frac{1}{1+d}} & -\sqrt{\frac{d}{1+d}} \end{bmatrix} \begin{pmatrix} b\vec{p}' \\ b\vec{p} \end{pmatrix}, \tag{B2}$$

with d as a yet undetermined parameter. A comparison with Eq. (B1) leads to

$$\begin{aligned}
\frac{b_\mathcal{K}}{2b} &= \sqrt{\frac{d}{1+d}} = \sqrt{\frac{1}{1+d}}, \\
\frac{b_q}{b} &= \sqrt{\frac{1}{1+d}} = \sqrt{\frac{d}{1+d}},
\end{aligned} \tag{B3}$$

which is then solved as

$$\begin{aligned}
d &= 1 \quad \text{and} \quad b_\mathcal{K} = \sqrt{2}b, \\
d &= 1 \quad \text{and} \quad b_q = \frac{b}{\sqrt{2}}.
\end{aligned} \tag{B4}$$

This transformation of the harmonic oscillator lengths is the same for the conjugate variables $\vec{\zeta}$ and $\vec{Z}$,

$$\begin{aligned}
d &= 1 \quad \text{and} \quad b_Z = \sqrt{2}b, \\
d &= 1 \quad \text{and} \quad b_\zeta = \frac{b}{\sqrt{2}}.
\end{aligned} \tag{B5}$$

The values of d enter the Talmi-Moshinsky brackets in Eq. (21), and b_q and $b_\mathcal{K}$ the radial oscillator functions.

APPENDIX C: DERIVATION OF THE CENTER-OF-MASS CONTRIBUTION

As indicated in Eq. (16), the variable ζ can be separated into a component representing the relative motion and one for the c.m. motion. The displacement Z is already translationally invariant. According to Eq. (13) the c.m. component of (SA-)NCSM eigenstates is exactly factorized and, by construction, is in the $|0s\rangle$ state. Thus we need to compute Eq. (24):

$$\begin{aligned}
\langle \phi_{\text{c.m.}} 0s | e^{-i\vec{q} \cdot \vec{\zeta}_{\text{c.m.}}} | \phi_{\text{c.m.}} 0s \rangle &= \int \int d^3 R_{\text{c.m.}} d^3 R'_{\text{c.m.}} R_{nl}(R_{\text{c.m.}}) R_{n'l'}(R'_{\text{c.m.}}) \mathcal{Y}_{K0}^{ll'}(\widehat{R_{\text{c.m.}}}, \widehat{R_{\text{c.m.}}}') e^{-i\vec{q} \cdot \vec{\zeta}_{\text{c.m.}}} \\
&= \int \int d^3 \zeta_{\text{c.m.}} d^3 Z_{\text{c.m.}} \sum_{n_q, n_K, l_q, l_\mathcal{K}} \langle n_\mathcal{K} l_\mathcal{K}, n_q l_q : K | n'l', nl : K \rangle_{d=1} R_{n_\zeta l_\zeta}(\zeta_{\text{c.m.}}) R_{n_Z l_Z}(Z_{\text{c.m.}} = 0) \\
&\quad \times \mathcal{Y}_{K0}^{l_\zeta l_Z}(\widehat{\zeta_{\text{c.m.}}}, \widehat{Z_{\text{c.m.}}}) e^{-i\vec{q} \cdot \vec{\zeta}_{\text{c.m.}}} \\
&= \int d^3 \zeta_{\text{c.m.}} R_{00}(\zeta_{\text{c.m.}}) R_{00}(0) \frac{1}{4\pi} e^{-i\vec{q} \cdot \vec{\zeta}_{\text{c.m.}}}.
\end{aligned} \tag{C1}$$

We note that

$$\langle n_\mathcal{K} = 0l_\mathcal{K} = 0, n_q = 0l_q = 0 : K = 0 | n' = 0l' = 0, n = 0l = 0 : K = 0 \rangle_{d=1} = 1. \tag{C2}$$

Furthermore, if $n = l = n' = l' = 0$, then $n_q = l_q = n_\mathcal{K} = l_\mathcal{K} = 0$ as well.

Evaluating the radial wave function using Eq. (A2) with the corresponding harmonic oscillator lengths, we obtain

$$R_{00}(\zeta_{\text{c.m.}}) = \left[\frac{2^2}{(b_{\zeta_{\text{c.m.}}}^2)^{3/2}\sqrt{\pi}}\right]^{\frac{1}{2}} e^{-\frac{1}{2}\frac{\zeta_{\text{c.m.}}^2}{b_{\zeta_{\text{c.m.}}}^2}}, \quad R_{00}(Z_{\text{c.m.}}=0) = \left[\frac{2^2}{(b_{Z_{\text{c.m.}}}^2)^{3/2}\sqrt{\pi}}\right]^{\frac{1}{2}}, \tag{C3}$$

where $b_{\zeta_{\text{c.m.}}}^2 = \frac{b_\zeta^2}{A}$ and $b_{Z_{\text{c.m.}}}^2 = \frac{b_Z^2}{A}$.

Inserting Eq. (C3) into Eq. (C1) leads to

$$\langle\phi_{\text{c.m.}}0s|e^{-i\vec{q}\cdot\vec{\zeta}_{\text{c.m.}}}|\phi_{\text{c.m.}}0s\rangle = \left(\frac{1}{\pi}\right)^{3/2}\frac{1}{(b_{\zeta_{\text{c.m.}}})^{3/2}}\frac{1}{(b_{Z_{\text{c.m.}}})^{3/2}}\int d^3\zeta_{\text{c.m.}}\, e^{-\frac{1}{2}\frac{\zeta_{\text{c.m.}}^2}{b_{\zeta_{\text{c.m.}}}^2}-i\vec{q}\cdot\vec{\zeta}_{\text{c.m.}}}. \tag{C4}$$

Completing the square in the integral leads to

$$\langle\phi_{\text{c.m.}}0s|e^{-i\vec{q}\cdot\vec{\zeta}_{\text{c.m.}}}|\phi_{\text{c.m.}}0s\rangle = \left(\frac{2b_{\zeta_{\text{c.m.}}}}{b_{Z_{\text{c.m.}}}}\right)^{3/2}e^{-\frac{1}{2}b_{\zeta_{\text{c.m.}}}^2 q^2} = e^{-\frac{1}{4A}b^2 q^2}, \tag{C5}$$

where we used the relations for b_ζ and b_Z from Eq. (B5) to arrive at the final expression for the c.m. contribution.

---

[1] D. R. Entem and R. Machleidt, Phys. Rev. C **68**, 041001 (2003).

[2] E. Epelbaum, Prog. Part. Nucl. Phys. **57**, 654 (2006).

[3] E. Epelbaum, H.-W. Hammer, and U.-G. Meissner, Rev. Mod. Phys. **81**, 1773 (2009).

[4] D. Langr, I. Simecek, P. Tvrdik, T. Dytrych, and J. P. Draayer, in *Proceedings of the Federated Conference on Computer Science and Information Systems (FEDCSIS), 2012* (IEEE, Piscataway, NJ, 2012), p. 545.

[5] M. Shao, H. Aktulga, C. Yang, E. Ng, P. Maris, and J. Vary, Comput. Phys. Commun. **222**, 1 (2018).

[6] H. M. Aktulga, C. Yang, E. G. Ng, P. Maris, and J. P. Vary, Concurrency Comput. Pract. Exp. **26**, 2631 (2014).

[7] M. Jung, E. H. Wilson, III, W. Choi, J. Shalf, H. M. Aktulga, C. Yang, E. Saule, U. V. Catalyurek, and M. Kandemir, in *Proceedings of the International Conference on High Performance Computing, Networking, Storage and Analysis, SC '13* (ACM, New York, 2013), pp. 75:1–75:11.

[8] P. Navratil, J. P. Vary, and B. R. Barrett, Phys. Rev. Lett. **84**, 5728 (2000).

[9] P. Navratil, J. P. Vary, and B. R. Barrett, Phys. Rev. C **62**, 054311 (2000).

[10] R. Roth and P. Navratil, Phys. Rev. Lett. **99**, 092501 (2007).

[11] B. Barrett, P. Navrátil, and J. Vary, Prog. Part. Nucl. Phys. **69**, 131 (2013).

[12] C. Stumpf, J. Braun, and R. Roth, Phys. Rev. C **93**, 021301 (2016).

[13] T. Dytrych, K. D. Launey, J. P. Draayer, P. Maris, J. P. Vary, E. Saule, U. Catalyurek, M. Sosonkina, D. Langr, and M. A. Caprio, Phys. Rev. Lett. **111**, 252501 (2013).

[14] K. D. Launey, T. Dytrych, and J. P. Draayer, Prog. Part. Nucl. Phys. **89**, 101 (2016).

[15] P. Navratil, R. Roth, and S. Quaglioni, Phys. Rev. C **82**, 034609 (2010).

[16] S. Quaglioni and P. Navratil, Phys. Rev. Lett. **101**, 092501 (2008).

[17] S. Quaglioni and P. Navratil, Phys. Rev. C **79**, 044606 (2009).

[18] J. Dohet-Eraly, P. Navrátil, S. Quaglioni, W. Horiuchi, and G. Hupin, in *Proceedings, 21st International Conference on Few-Body Problems in Physics (FB21)*, Chicago, May 18–22, 2015 [EPJ Web Conf. **113**, 06002 (2016)].

[19] J. Rotureau, P. Danielewicz, G. Hagen, F. M. Nunes, and T. Papenbrock, Phys. Rev. C **95**, 024315 (2017).

[20] H. F. Arellano, F. A. Brieva, and W. G. Love, Phys. Rev. C **42**, 652 (1990).

[21] R. Crespo, R. C. Johnson, and J. A. Tostevin, Phys. Rev. C **46**, 279 (1992).

[22] C. Elster, S. P. Weppner, and C. R. Chinn, Phys. Rev. C **56**, 2080 (1997).

[23] P. Navrátil, S. Quaglioni, I. Stetcu, and B. R. Barrett, J. Phys. G: Nucl. Part. **36**, 083101 (2009).

[24] A. M. Shirokov, A. I. Mazur, S. A. Zaytsev, J. P. Vary, and T. A. Weber, Phys. Rev. C **70**, 044005 (2004).

[25] A. M. Shirokov, J. P. Vary, A. I. Mazur, S. A. Zaytsev, and T. A. Weber, Phys. Lett. B **621**, 96 (2005).

[26] J. Suhonen, *From Nucleons to Nucleus: Concepts of Microscopic Nuclear Theory* (Springer, Berlin, 2007).

[27] P. Rocheford and J. Draayer, Ann. Phys. (N.Y.) **214**, 341 (1991).

[28] B. Mihaila and J. H. Heisenberg, Phys. Rev. C **60**, 054303 (1999).

[29] P. Navratil, Phys. Rev. C **70**, 014317 (2004).

[30] C. Cockrell, J. P. Vary, and P. Maris, Phys. Rev. C **86**, 034325 (2012).

[31] T. Dytrych, A. C. Hayes, K. D. Launey, J. P. Draayer, P. Maris, J. P. Vary, D. Langr, and T. Oberhuber, Phys. Rev. C **91**, 024326 (2015).

[32] J. F. Berger, M. Girod, and D. Gogny, Nucl. Phys. A **502**, 85 (1989).

[33] D. G. J. F. Berger, M. Girod, Comput. Phys. Commun. **63**, 365 (1991).

[34] C. R. Chinn, C. Elster, R. M. Thaler, and S. P. Weppner, Phys. Rev. C **52**, 1992 (1995).

[35] G. P. Kamuntavicius, R. K. Kalinauskas, B. R. Barrett, S. Mickevicius, and D. Germanas, Nucl. Phys. A **695**, 191 (2001).

[36] M. Moshinsky and Y. Smirnov, *The Harmonic Oscillator in Modern Physics*, Contemporary Concepts in Physics (Harwood Academic, Reading, UK, 1996).

[37] T. Dytrych, P. Maris, K. D. Launey, J. P. Draayer, J. P. Vary, D. Langr, E. Saule, M. A. Caprio, U. Catalyurek, and M. Sosonkina, Comput. Phys. Commun. **207**, 202 (2016).

[38] P. Maris and J. P. Vary, Int. J. Mod. Phys. E **22**, 1330016 (2013).

[39] P. Maris, J. P. Vary, and A. M. Shirokov, Phys. Rev. C **79**, 014308 (2009).

[40] S. A. Coon, M. I. Avetian, M. K. G. Kruse, U. van Kolck, P. Maris, and J. P. Vary, Phys. Rev. C **86**, 054002 (2012).

[41] S. N. More, A. Ekström, R. J. Furnstahl, G. Hagen, and T. Papenbrock, Phys. Rev. C **87**, 044326 (2013).

[42] K. A. Wendt, C. Forssén, T. Papenbrock, and D. Sääf, Phys. Rev. C **91**, 061301 (2015).

[43] R. J. Furnstahl, G. Hagen, and T. Papenbrock, Phys. Rev. C **86**, 031301 (2012).

[44] A. Ekström, G. Baardsen, C. Forssén, G. Hagen, M. Hjorth-Jensen, G. R. Jansen, R. Machleidt, W. Nazarewicz, *et al.*, Phys. Rev. Lett. **110**, 192502 (2013).